RSC Advances

PAPER

View Article Online
View Journal | View Issue

Cite this: *RSC Adv.*, 2019, **9**, 2731

Structural growth pattern of neutral and negatively charged yttrium-doped silicon clusters $YSi_n^{0/-}$ (n=6–20): from linked to encapsulated structures†

Yuming Liu,[a] Jucai Yang,*[ab] Suying Li[b] and Lin Cheng *[a]

A global search for the low energy of neutral and anionic doped Si clusters $YSi_n^{0/-}$ (n = 6–20) was performed using the ABCluster global search technique coupled with a hybrid density functional method (mPW2PLYP). In light of the calculated energies and the measured photoelectron spectroscopy values, the true minima of the most stable structures were confirmed. It is shown that the structural growth pattern of YSi_n^- (n = 6–20) is from Y-linked two subcluster structure to a Y-encapsulated structure in Si cages, while that of YSi_n (n = 6–20) is from substitutional to linked structures, and as the number of Si atoms increases, it evolves toward the encapsulated structure. Superatom YSi_{20}^- with a high-symmetry endohedral I_h structure has an ideal thermodynamic stability and chemical reactivity, making it the most suitable building block for novel optical, optoelectronic photosensitive or catalytic nanomaterials.

Received 19th November 2018
Accepted 3rd January 2019

DOI: 10.1039/c8ra09492f

rsc.li/rsc-advances

Introduction

Rare-earth metal silicides as novel functional materials have been extensively used in various fields such as microelectronics and optical instruments due to their remarkable magnetic, electrical, and optical properties and their chemical stabilities.[1–3] For instance, silicon is a poor photonic material owing to its very short non-radiative lifetime and indirect band gap, but introducing erbium to a silicon microcrystal can be used as a silicon based optical source.[4] Yttrium silicides are ideal in devices such as large scale integrated circuits, infrared detectors, ohmic contacts and rectifying contacts because the interfaces of yttrium and silicon have very small lattice mismatches, sharp interfaces, high conductivity, low Schottky barrier heights and very good thermal stability.[5,6] In the past few decades, a great deal of research on yttrium silicide has been performed. These studies focus mainly on the formation of amorphous yttrium silicide and have proposed that nanoclusters play a role in such physical and chemical processes. Nanoclusters have been one of the central issues of nanomaterial sciences because of their unique structures and properties.[7–10] Consequently, it is very important to probe the evolution of yttrium silicide aggregates in the transition from the molecular to the condensed phase.

Several efforts have been made in the past decade to study the structural and electronic properties of yttrium doped silicon clusters.[11–17] The structures, stabilities and electronic properties of small-sized YSi_n (n = 1–6) were evaluated by using single-hybrid B3LYP density functional.[11,12] Ren and co-workers[13] probed the geometries and electron properties of YSi_n with n up to 16 by means of a relativistic density functional investigation and concluded that (i) the spin–orbit correction is small and negligible; (ii) the most stable structures keep analogous frameworks to the Si_{n+1} cluster for n = 1–14, but encapsulated geometries starting from n = 15. For anions, silicon clusters doped with yttrium atoms, YSi_n^- (n = 6–20) were generated by a double-laser vaporization technique and their electronic and geometric stabilities were characterized with adsorption reactivity and photoelectron spectroscopy (PES).[2,3] In addition, the structure of the YSi_n^- clusters was deduced by a chemical probe method,[2,3] and it was found that the YSi_n^- clusters evolved from incomplete cage-type structures to cage-type structures from n = 16 to n = 20.[2,3] After these experiments, a simulated annealing approach combined with a B3PW91 theoretical simulation for YSi_n^- (n = 4–20) was achieved by Jaiswal *et al.*[17] They found that YSi_{16}^-, YSi_{17}^- and YSi_{20}^- adopt the cage structures and YSi_{18}^- and YSi_{19}^- adopt the linked structures. Obviously, this growth behavior is different from that of the experimental results.[2,3]

Although these theoretical studies concentrated on the structural stability and evolution of yttrium-doped neutral and anionic Si_n ($n \leq 20$) clusters and provided important information for further theoretical and experimental research, some questions still remain open in yttrium-doped silicon clusters: (i)

[a]*School of Chemical Engineering, Inner Mongolia University of Technology, Inner Mongolia Key Laboratory of Theoretical and Computational Chemistry Simulation, Hohhot 010051, People's Republic of China. E-mail: lcheng1983@aliyun.com; yangjc@imut.edu.cn*

[b]*School of Energy and Power Engineering, Inner Mongolia University of Technology, Hohhot 010051, People's Republic of China*

† Electronic supplementary information (ESI) available. See DOI: 10.1039/c8ra09492f

the functional dependence on the predicted lowest-energy structure may occur for small- or medium-clusters, especially for species including rare earth- or transition-metal atoms. Therefore, the choice of calculation method is very important.[18] Based on our previous studies about REM-doped Si clusters (REM = Sm, Eu Gd, Ho, Pr),[19–24] compared to the pure or single-hybrid density functional (such as PBE, B3LYP, PBE0, TPSSh, wB97X, and wB97XD), the adiabatic electron affinities (AEAs) calculated at the B2PLYP and mPW2PLYP level show a better comparison with the experimental information. In addition, the theoretical and experimental photoelectron spectroscopy (PES) spectra are in good agreement at the mPW2PLYP and the B2PLYP level.[19,22,23] (ii) It is possible to leave out the most stable structure during the initial configuration selection without a global search technique.[25,26,27] For small-sized clusters, the global optimization approach is a very effective method and can completely solve the problem of ground state structure loss. Without doubt it is impossible to make an "ergodic" sampling on the potential energy surface of large clusters by a global search technique. Consequently, it is reasonable and necessary to take into account a substitutional structure (this can be regarded as replacing a Si atom of Si_{n+1} with a metal atom), an attaching structure (this can be viewed as adding a metal atom to the Si_n geometry) and so on as a complement to the global search method. (iii) A detailed comparison of the theoretical and experimental results, such as PES, infrared or Raman spectra, is the most effective strategy because there is no experimental method for directly measuring the most stable structure of clusters so far. (iv) As the diversity of the properties of Y-doped Si clusters can hardly be explained without understanding the structural evolution patterns, in this paper the ABCluster global search technique combined with a double-hybrid density functional scheme was adopted for the geometry optimization of neutral and anionic Y-doped Si_n (n = 6–20) clusters with the aim of elucidating the structural evolution pattern of their ground states, studying their electronic properties, understanding their bonding characteristics, and providing significant information for further theoretical and experimental explorations of semiconductor clusters doped with other transition or rare-earth metals. Good agreement between the theoretical and experimental data, including PES, vertical detachment energy (VDE) and adiabatic electron affinity (AEA), strongly supports the validity of our global minimum geometries.

Computational details

To search for the most stable structure for YSi_n (n = 6–20) and their anions, three techniques were adopted to search their initial configurations. First, we use the free program "ABCluster" to perform the global search.[28] The ABCluster program uses the artificial bee colony (ABC) algorithm to conduct the global search for clusters. Initially, we used the ABCluster program generating 300 cluster structures for $YSi_n^{0/-}$ (n = 6–20) at the PBE/BSI level (BSI: Si: 6-31G; Y: LANL2DZ).[29,30] Then, the isomers with an energy difference within 0.8 eV of the lowest energy clusters were selected and re-optimized at the PBE/BSII level (BSII: Si: cc-pVTZ; Y: SDD).[31–33] Second, the substitutional structures were collected, in which a Si atom in the most stable structure of Si_{n+1} was replaced with a Y atom. Third, isomers already presented in the preceding literature[13,17] were adopted. Vibrational frequency calculations were carried out at the same level to assure the nature of the stationary points. After completion of the initial geometry optimization by PBE, we selected, again, the low-lying isomers and reoptimized them by means of a double hybrid mPW2PLYP functional[34] at the same level. Vibrational frequency was not carried out at the mPW2PLYP level. In order to further refine the energies, single-point energy calculations were carried out at the mPW2PLYP level with the aug-cc-pVTZ basis set[33] for Si atoms (basis set for Y atoms unchanged). According to Koopmans' theorem,[35,36] we simulated the PES spectra of anionic species at the mPW2PLYP level with the Multiwfn program[37] and compared them with the experimental PES spectra. In light of the adaptive natural density partitioning (AdNDP),[38] chemical bonding analyses were performed to gain chemical insight. To further understand the interaction between the Y atom and silicon clusters, natural population analyses (NPA) were also performed. We also performed the calculations with an all-electron basis set for Y atoms (in optimization an all-electron TZP basis set[39] was substituted for the effective core potentials SDD basis set,[31,32] and in single-point energy calculation the aug-TZP basis set[39] was substituted for the SDD basis set) and compared these with SDD basis set calculations. The results revealed that the SDD Y–Si bond distances are averagely longer than those of the all-electron TZP basis set by 0.021 Å (see Fig. S1 in ESI†), and the mean absolute deviations of AEA and VDE between SDD and the all-electron TZP basis set are only 0.02 eV. Consequently, the results calculated with the SDD basis set for Y should be reliable and the discussions below are based on the SDD results. All of the calculations were implemented using the GAUSSIAN 09 package.[40]

Results and discussion

The most stable structures

The most stable structures of $YSi_n^{0/-}$ (n = 6–20) clusters are displayed in Fig. 1 and 2. The corresponding low-lying isomers, relative energies and point groups are displayed in Fig. S2 and S3 (in ESI†). The electronic state, HOMO–LUMO energy gap, average binding energies, and NPA charges on the Y atom for the most stable structure are summarized in Table 1. For anionic clusters, the calculated spin states of YSi_n^- ($n \leq 20$) are single with the exception of YSi^- and YSi_2^- which are triplet. For neutral clusters, the predicted spin states are single excluding YSi, which is quartet.

The structural evolution of the anionic yttrium doped silicon clusters is from the linked to encapsulated configurations based on our results of ABCluster global search technique combined with the double-hybrid density functional scheme. The most stable structure is a pentagonal bipyramid for n = 6 and a bi-face-capped tetragonal bipyramid for n = 7. For n = 8–15, the most stable structure is linked configurations excluding YSi_9^- which is a bi-face-capped (one of them is

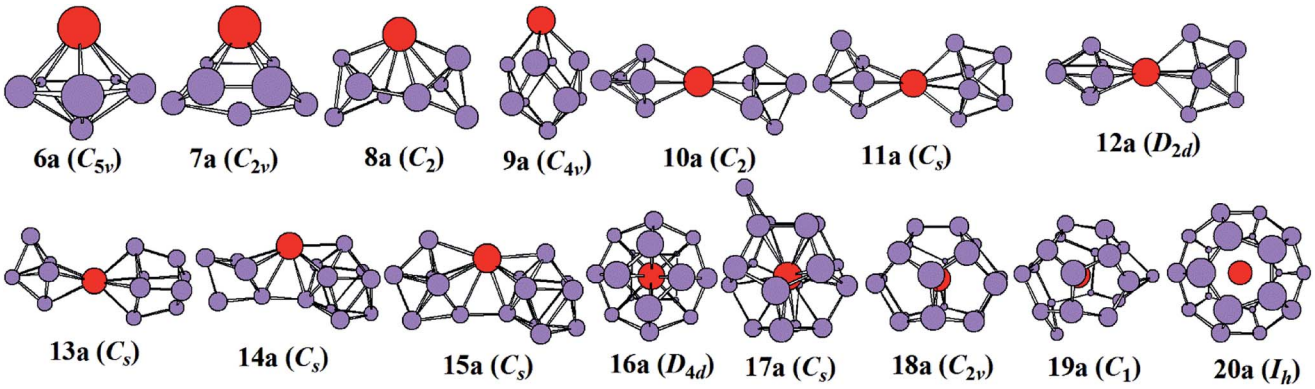

Fig. 1 The most stable structures of YSi_n^- (n = 6–20) and their point groups.

a Y atom) tetragonal antiprism. The Y atom in YSi_8^- links two subclusters of Si_4 tetrahedrons, that in YSi_{10}^- links two orthogonal subclusters of a Si_5 trigonal bipyramid, that in YSi_{11}^- links a Si_5 trigonal bipyramid and a Si_6 capped trigonal bipyramid, that in YSi_{12}^- links two orthogonal subclusters of a Si_6 capped trigonal bipyramid, that in YSi_{13}^- links a Si_5 trigonal bipyramid and a Si_8 distorted bicapped octahedron, that in YSi_{14}^- links a Si_5 trigonal bipyramid and a tricapped trigonal prism (TTP) Si_9 motif, and that in YSi_{15}^- links a Si_6 capped trigonal bipyramid and a Si_9 TTP subcluster. For n = 16–20, the most stable structure is the encapsulated configuration with the Y atom centering in the Si cage. The most stable structures of YSi_{16}^- and YSi_{20}^- are high-symmetry fullerene-like D_{4d} and I_h, respectively, endohedrons. The most stable structure of YSi_{17}^- can be viewed as capping a Si atom to the ground state structure of YSi_{16}^-. The most stable structures of YSi_{18}^- and YSi_{19}^- can be regarded as removing one and two Si atoms from the ground state structure of YSi_{20}^-, respectively. These results are different from the previously reported linked structures.[17] For anionic yttrium doped Si clusters, the most stable YSi_n^- (n = 7, 10–14) structures reported in ref. 15 correspond to 7a3, 10a3, 11a5, 12a5, 13a2, and 14a3 in Fig. S2.† As shown in Fig. S2,† their energies are about 0.04–1.09 eV higher than those of the corresponding most stable structures in our work.

The structural evolution of the neutral YSi_n (n = 6–20) from substitutional structures to linked configurations and finally to an encapsulated fullerene-like motif occurs at n = 14 and 16, respectively. For n = 6–13, the most stable structures differ from those of the corresponding anions, and they belong to substitutional structures with the exception of YSi_7, which is a face-capped pentagonal bipyramid and is only more stable in energy than the substitutional structure 7n2 (in Fig. S3 of ESI†) by 0.02 eV. The most stable structures of YSi_6, YSi_8, YSi_9, YSi_{10}, YSi_{11}, YSi_{12}, and YSi_{13} can be viewed as the most stable structures of the Si_7 pentagonal bipyramid,[41] Si_9 distorted bicapped pentagonal bipyramid,[40] Si_{10} tetracapped trigonal prism,[41–43] Si_{11} pentacapped trigonal prism,[43] Si_{12} hexacapped trigonal prism,[44] Si_{13} (a distorted TTP with an additional rhombus capped on one edge of the prism) and Si_{14} (two stacked rhombi with distortion and one fivefold ring capped with an atom),[44] respectively, with a Si atom replaced by a Y atom. For n = 14 and 15, the most stable configurations are analogous to those of their anions, in other words, linked structures. As for n = 16–20, their most stable structures are an encapsulated configuration with the Y atom located at the center of the Si cage. The ground

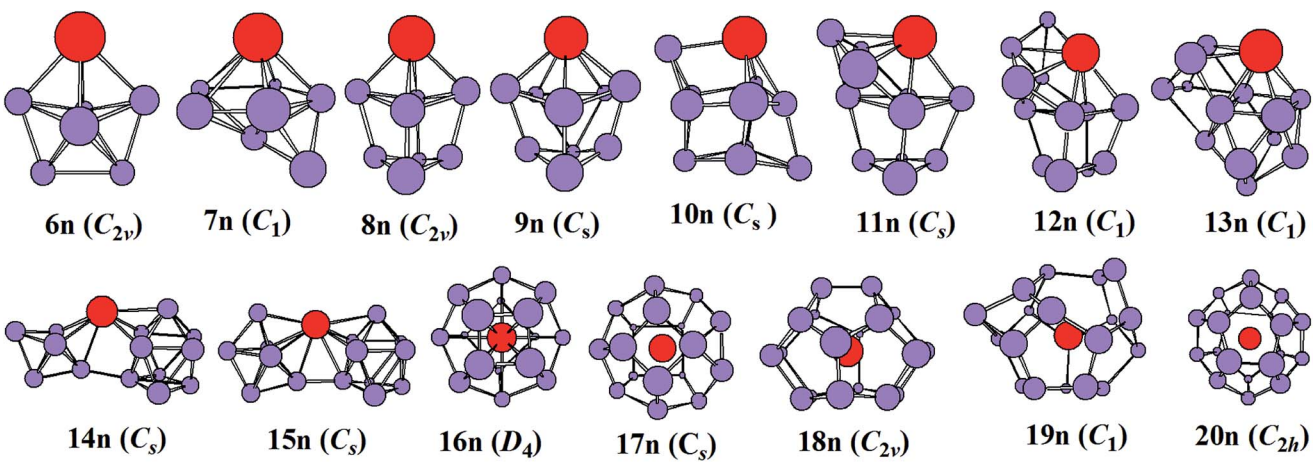

Fig. 2 The most stable structures of YSi_n (n = 6–20) and their point groups.

Table 1 Electronic state, average bonding energy E_b (eV), HOMO–LUMO energy gap E_{gap} (eV), and the charge on the Y atom Q(Y) (a.u.) of the most stable structures of $YSi_n^{0/-}$ (n = 6–20) clusters

	YSi_n^-				YSi_n			
n	State	E_b	E_{gap}	Q(Y)	State	E_b	E_{gap}	Q(Y)
6	$^1A_1$	4.36	3.51	0.52	$^2A_1$	4.25	3.73	0.71
7	$^1A_1$	4.42	3.30	0.34	^2A	4.28	3.76	0.70
8	^1A	4.52	3.32	0.43	$^2A_1$	4.38	2.86	0.72
9	$^1A_1$	4.62	3.07	0.55	$^2A'$	4.46	3.63	0.69
10	^1A	4.63	4.59	0.44	$^2A'$	4.48	3.31	0.71
11	$^1A'$	4.66	4.50	0.19	$^2A'$	4.52	3.35	0.46
12	$^1A_1$	4.68	4.48	−0.13	^2A	4.54	3.43	0.28
13	$^1A'$	4.69	4.44	0.03	^2A	4.57	3.31	0.62
14	$^1A'$	4.73	3.73	0.21	$^2A'$	4.60	4.19	0.42
15	$^1A'$	4.73	3.47	−0.07	$^2A'$	4.61	4.00	0.10
16	$^1A_1$	4.78	3.58	−3.38	$^2B_2$	4.63	3.50	−3.36
17	$^1A'$	4.74	3.19	−3.33	$^2A'$	4.61	2.84	−3.19
18	$^1A_1$	4.79	2.30	−2.82	$^2A_1$	4.68	2.61	−2.93
19	^1A	4.78	2.50	−2.93	^2A	4.67	2.73	−3.00
20	^1A_g	4.89	2.48	−2.57	^2A_u	4.76	2.39	−2.88

state structures of YSi_{16} and YSi_{20} are slightly distorted and of reduced symmetries compared with those of the corresponding anions. The most stable configurations of YSi_{18} and YSi_{19} are similar to those of their anions, while the most stable structure of YSi_{17} is different from that of its anion. It is noted that the most stable structures of YSi_{13}, YSi_{14} and YSi_{15} presented in this work differ from those reported previously.[13] The most stable YSi_n (n = 13–15) structures reported in ref. 11 correspond to 13n5, 14n3 and 15n2 in Fig. S3† of our work. As shown in Fig. S3,† their energies are about 0.32–0.89 eV higher than those of the corresponding most stable structures in our work.

Photoelectron spectroscopy (PES) of anionic clusters

It is necessary to verify the validity of the predicted most stable structures. It is known that PES is a significant technology to extract conformational fingerprints from the ground state structures, which can provide more information about the underlying electronic structures. Therefore, the validity of the predicted most stable structures can be tested by means of comparing their theoretical and experimental PES spectra. We used two criteria in comparing the theoretical results with the experimental data: (i) AEA and first VDE and (ii) the number of different peaks and their relative position in the low-binding-energy portion of the PES spectra. The simulated PES spectra of the lowest-energy structures coupled with the experimental PES spectra are pictured in Fig. 3. The calculated first VDE are summarized in Table 2 along with experimental data. It can be seen from the simulated PES of YSi_6^- that there are three major peaks (X, A, and B) located at 3.18, 4.44, and 5.41 eV, which are in excellent agreement with the three peaks of 3.25, 4.50, and 5.40 eV observed in the experimental research.[2] The simulated PES of YSi_7^- also has three peaks (X, A, and B) located at 2.86, 4.52, and 5.66 eV, which match the experimental data of 3.10, 4.40 and 5.70 eV.[2] For YSi_8^-, four discrete peaks (X, A–C) centered at 2.98, 3.56, 4.41, and 5.31 eV are obtained and they agree with the experimental values of 3.25, 3.70, 4.40, and 5.30 eV,[2] especially for the latter three peaks. For YSi_9^-, two peaks (X and A) of 3.23 and 4.38 eV are in concord with experimental data of 3.40 and 4.40 eV.[2] For YSi_{10}^-, there are three distinct peaks (X, A, and B) centered at 4.10, 5.05 and 5.30 eV, which reproduce well the experimental values of 4.20, 4.90 and 5.20 eV.[2] Unfortunately, the simulated and experimental PES spectra[2] of YSi_{11}^- have large differences. There are three peaks (X, A, and B) located at the simulated PES, while only two peaks are observed in the experimental PES. The first peak (X) located at 3.81 eV does not match the experimental value of 4.20 eV. For YSi_{12}^-, the first three distinct peaks (X, A, and B) centered at 3.57, 4.42 and 5.14 eV are close to the experimental data of 3.70, 4.60 and 5.40 eV.[2] The simulated PES of YSi_{13}^- yields two major peaks (X and A) at 4.33 and 5.23 eV, in excellent agreement with the experimental data of 4.30 and 5.10 eV.[2] The first two peaks (X and A) located at 3.65 and 4.17 eV for YSi_{14}^- are very close to the experimental data of 3.75 and 4.20 eV.[2] For n = 15–18 and 20, their first three peaks (X, A, and B) located, respectively, at 3.46, 4.08 and 4.88 eV, 4.00, 5.01 and 5.45 eV, 4.04, 5.10 and 5.83 eV, 3.92, 4.75 and 5.24 eV, and 4.28, 5.29 and 5.98 eV reproduce well those of experiments.[2] The three peaks (X, A and B located at 4.40, 5.00 and 5.40 eV) of the experimental spectra of YSi_{19}^- are almost simulated by the calculations with a shift of the first three peaks (X, A and B centered at 3.60, 4.26 and 4.72 eV) to a higher binding energy. In addition to YSi_{11}^- and YSi_{19}^-, quantitative analyses revealed that the mean absolute error of the calculated first VDEs of YSi_n^- (n = 6–10, 12–18, 20) from the experimental data are 0.15 eV. Good agreement between the theoretical and experimental PES spectra sheds further light on the validity of the predicted global minimum structures. Based on our reliable theoretical predictions, we suggest that the experimental PES of the YSi_{11}^- cluster should be checked further.

AEA is defined as the energy difference in the manner:[19]

$$\mathrm{AEA} = E_{\mathrm{neutral}} - E_{\mathrm{anion}} + \Delta E_{\mathrm{sc}} \quad (1)$$

where $E_{neutral}$ and E_{anion} are the most stable energy of the neutral and anionic species, respectively, and ΔE_{sc} is the structural correction factor related to the charge of rare-earth atom in the anion clusters. As an empirical correction, the values of ΔE_{sc} are assigned to be 0.00, −0.20 and −0.40 eV for no-cage, half-cage, and cage structures, respectively. As seen in Table 1, the NPA charges on the Y atom are positive or slightly negative when n = 6–15, while they are negatively charged when n = 16–20. Therefore, the $YSi_n^{-/0}$ clusters (n = 6–15) are no-cage structures, while the $YSi_n^{-/0}$ clusters (n = 16–20) are cage structures. This empirical correction, ΔE_{sc}, has been successfully used in the $ScSi_n^{-/0}$ clusters in ref. 19. Since the radius of the Y atom is larger than that of the Sc atom,[19] the Y-doped silicon clusters do not appear as the half-cage like the Sc-doped silicon clusters. Therefore, the ΔE_{sc} for YSi_n^- with n = 6–15 is 0.00 eV, and −0.40 eV for n = 16–20. The theoretical and experimental AEA are listed in Table 2. It can be seen from Table 2 that the theoretical AEAs of YSi_n (n = 7–9, 11–15, 17–19) are in good concord with the experimental data. The mean absolute

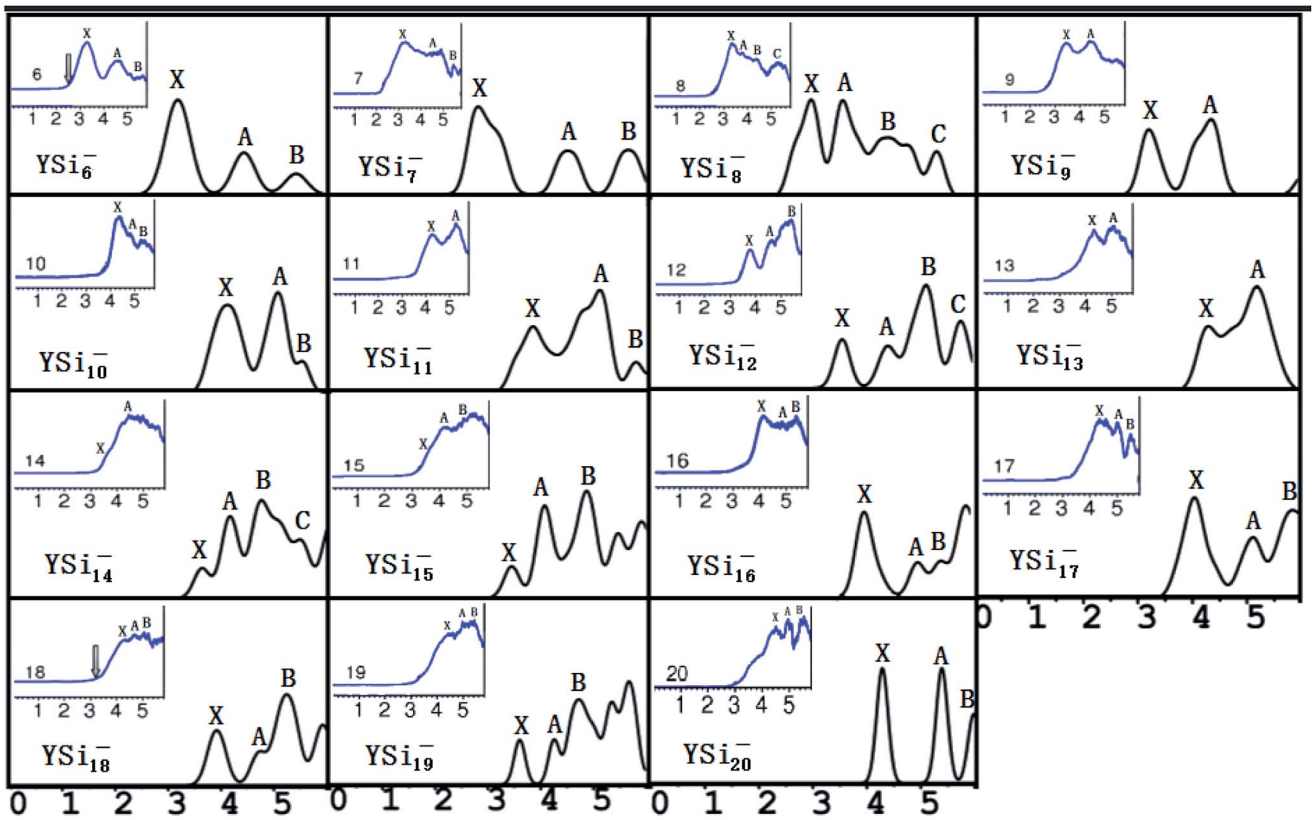

Fig. 3 Simulated PES spectra of the ground state YSi_n^- (n = 6–20) species. The insets show experimental PES spectra.[2]

errors are by 0.15 eV. The deviation of the theoretical and experimental AEA for n = 6, 10, 16 and 20 may be attributed to their PES with a long round tail without obvious features, which makes it difficult to determine the precise experimental AEA. Taking YSi_{16}^- as an example, the spectral diagram of the redistributed AEA is given in Fig. S4 (ESI†), where the black arrow corresponds to the original assigned AEA,[2] and the red dashed line corresponds to the newly allocated AEA. It is obvious that the dot corresponding to the red dashed line as the threshold is more reasonable than the dot corresponding to the black arrow as the threshold. That is, the experimental AEA value may be 3.50 ± 0.10 eV, but not 2.97 ± 0.15 eV (ref. 3) or 3.20 ± 0.004 eV.[2] The good agreement between the calculated and experimental AEAs supports the validity of the predicted most stable structure for neutral YSi_n. Among all of these AEAs, the theoretical AEA of YSi_{20}^- is the maximum (3.83 eV), which indicates that the YSi_{20}^- cluster has a high stability.

Table 2 The theoretical and experimental adiabatic electron affinity (AEA) and first vertical detachment energy (VDE) for YSi_n^- (n = 6–20)

	VDE			AEA		
n	Theor.	Exp.	Δ_{VDE}[b]	Theor.	Exp.	Δ_{AEA}[b]
6	3.18	3.25 ± 0.1[a]	0.07	2.16	2.50 ± 0.004[a]	0.34
7	2.86	3.10 ± 0.1[a]	0.24	2.41	2.20 ± 0.004[a]	−0.21
8	2.98	3.25 ± 0.1[a]	0.27	2.63	2.60 ± 0.004[a]	−0.03
9	3.23	3.40 ± 0.1[a]	0.17	2.95	2.70 ± 0.004[a]	−0.25
10	4.10	4.20 ± 0.1[a]	0.10	3.00	3.60 ± 0.004[a]	0.60
11	3.81	4.20 ± 0.1[a]	0.39	3.09	3.30 ± 0.004[a]	0.21
12	3.57	3.70 ± 0.1[a]	0.13	3.27	3.20 ± 0.004[a]	−0.07
13	4.33	4.30 ± 0.1[a]	−0.03	3.06	3.00 ± 0.004[a]	−0.06
14	3.65	3.75 ± 0.1[a]	0.10	3.31	3.10 ± 0.004[a]	−0.21
15	3.46	3.60 ± 0.1[a]	0.14	3.30	3.10 ± 0.004[a]	−0.20
16	4.00	4.10 ± 0.1[a]	0.10	3.50	3.20 ± 0.004[a]	−0.30
17	4.04	4.20 ± 0.1[a]	0.16	3.27	3.20 ± 0.10[a]	−0.07
18	3.92	4.20 ± 0.1[a]	0.28	3.08	3.10 ± 0.004[a]	0.02
19	3.60	4.40 ± 0.1[a]	0.80	3.05	3.20 ± 0.004[a]	0.15
20	4.28	4.40 ± 0.1[a]	0.12	3.83	3.00 ± 0.004[a]	−0.83

[a] Ref. 2. [b] Δ = theor. − exp.

Relative stability

Two important parameters related to thermodynamic and relative stability, atomization energy (AE) and second energy difference (Δ^2E), were examined for the determined global minimum structures of $YSi_n^{0/-}$ (n = 6–20) clusters. The AE is the energy required for the following reactions:

$$YSi_n \rightarrow nSi + Y \quad (2)$$

$$YSi_n^- \rightarrow (n-1)Si + Si^- + Y \quad (3)$$

Δ^2E refers to the following reactions:

$$2YSi_n \rightarrow YSi_{n+1} + YSi_{n-1} \quad (4)$$

$$2YSi_n^- \rightarrow YSi_{n+1}^- + YSi_{n-1}^- \quad (5)$$

The predicted AE and Δ^2E are sketched in parts (a) and (b) of Fig. 4, respectively. From Fig. 4a we can conclude that (i) the AE data of the anionic clusters are all larger than those of corresponding neutral clusters in respect that the YSi_n species are open-shell electronic configurations, while the YSi_n^- clusters are closed-shell electronic configurations which minimize the electronic repulsions in light of the Pauli exclusion principle. The larger the values of AE, the higher the relative stabilities; (ii) Starting from $n = 12$ for anionic clusters and $n = 14$ for neutral clusters, the cluster size distributions exhibit even–odd alternations. An even number of Si atoms is are more stable than those with an odd number. And the even–odd alternations are more and more obvious from the linked motif to the encapsulated configuration. This conclusion is clearly reproduced in Fig. 4b because the Δ^2E is a susceptive survey for relative stability. The HOMO–LUMO energy gap is a significant physical parameter can be regarded as an indicator of chemical reactivity. The larger the HOMO–LUMO energy gap, the weaker the chemical reactivity. Fig. 4c pictures the HOMO–LUMO energy gaps of $YSi_n^{0/-}$ (n = 6–20) clusters. From Fig. 4c the odd–even oscillation behavior is not observed for the clusters. For YSi_n^-, the HOMO–LUMO energy gaps of n = 10–13 are relatively large and range from 4.44 to 4.59 eV, which broaden the HOMO–LUMO energy gaps of the corresponding anionic Si_n^- clusters (for the values for Si_n^- see ref. 17). The rest of the Y-doped anionic Si_n^- clusters narrow the HOMO–LUMO energy gap. For n = 18–20, their HOMO–LUMO energy gaps are relatively small and range from 2.30 to 2.50 eV, which indicates that they have good chemical activity and are beneficial to the preparation of novel functional materials, such as optical and optoelectronic photosensitive materials or catalytic materials, especially so for YSi_{20}^-, which possesses a good thermodynamic stability, as discussed above. For neutral YSi_n, Y-doped Si_n clusters narrow the HOMO–LUMO energy gap. The HOMO–LUMO energy gaps for n = 14 and 15 are relatively large, and relatively small for n = 8, 17–20. The HOMO–LUMO energy gap of neutral YSi_{20} is very close to that of the corresponding anion, showing that an extra electron does not change the chemical reactivity, but improves the thermodynamic stability.

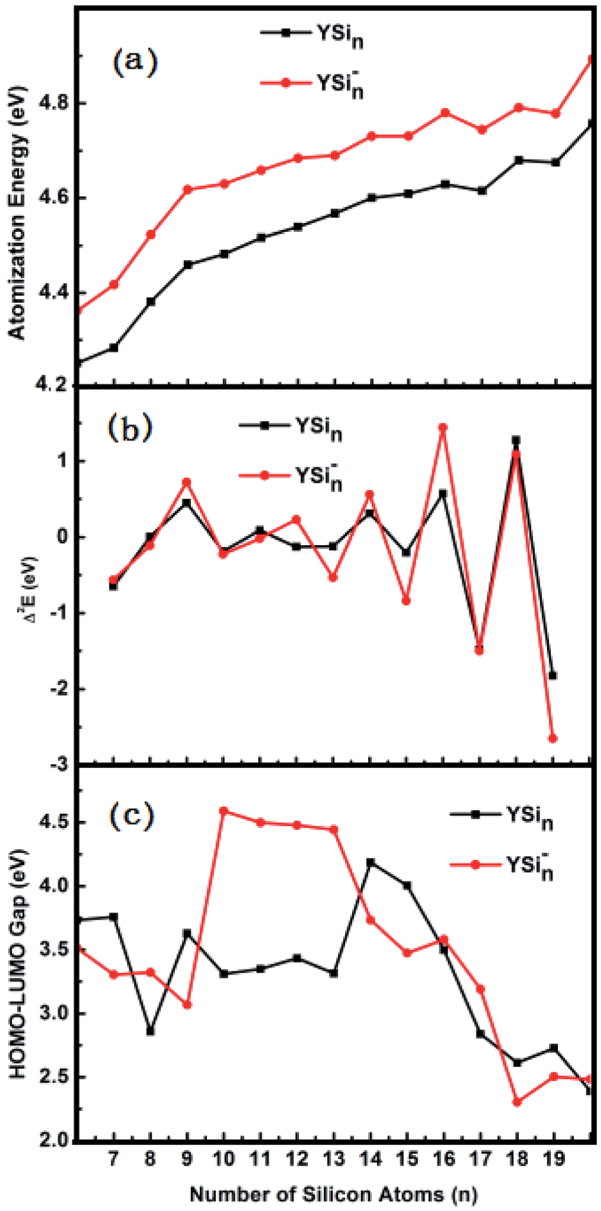

Fig. 4 Size dependences of (a) atomization energy (AE), (b) second energy difference (Δ^2E), and (c) HOMO–LUMO energy gap for the most stable YSi_n^- (n = 6–20) clusters.

Chemical bonding analysis

To gain an in-depth understanding of the ideal thermodynamic stability and chemical reactivity of anionic YSi_{20}^-, the molecular orbitals (MOs), as plotted in Fig. 5, are firstly analyzed. Based on the spherical jellium model and the MO energies, the electronic shells for superatom YSi_{20}^- with the magic number of 84 valence electrons are best described as $1S^21P^61D^{10}1F^{14}1G^82S^21G^{10}2P^62D^{10}3S^22F^{14}$, in which the 1S jellium model shell features σ bonds between the s-orbitals of the peripheral Si atoms and the centric Y atom. The 2S and 3S features π and π + δ bonds between the p-orbitals of the peripheral Si atoms and the d-orbital of the nuclear Y atom, respectively. Both 1P and 2P jellium model shells are threefold degenerate, and are characterized with π orbitals primarily originating from Si 3p and Y 4d. Both 1D and 2D jellium model shells are fivefold degenerate, and are σ + π bonds formed mainly by s- and p-orbitals of the peripheral Si atoms. The 1F, 1G, and 2F, excluding HOMO−3, HOMO−4, HOMO−5 and HOMO−6, are also σ + π bonds formed primarily by s- and p-orbitals of the Si atoms. The occupied MOs HOMO−3, HOMO−4, HOMO−5 and HOMO−6 are fourfold degenerate, and characterized with π + δ bonds mainly derived from 3p orbitals of the peripheral Si atoms and 4d orbitals of the centric Y atom. Through the above analyses, we can find that (i) the high occupied orbitals degeneracy may be attributed to the high symmetry I_h of the YSi_{20}^- clusters; and (ii) the 4d orbitals of the Y atom have significant contributions to the occupied MOs and reinforce the interactions between the outer fullerene Si_{20} cage and the nuclear Y atom. Secondly, the AdNDP method[36] is was employed to perform a quantitative insight into the nature of

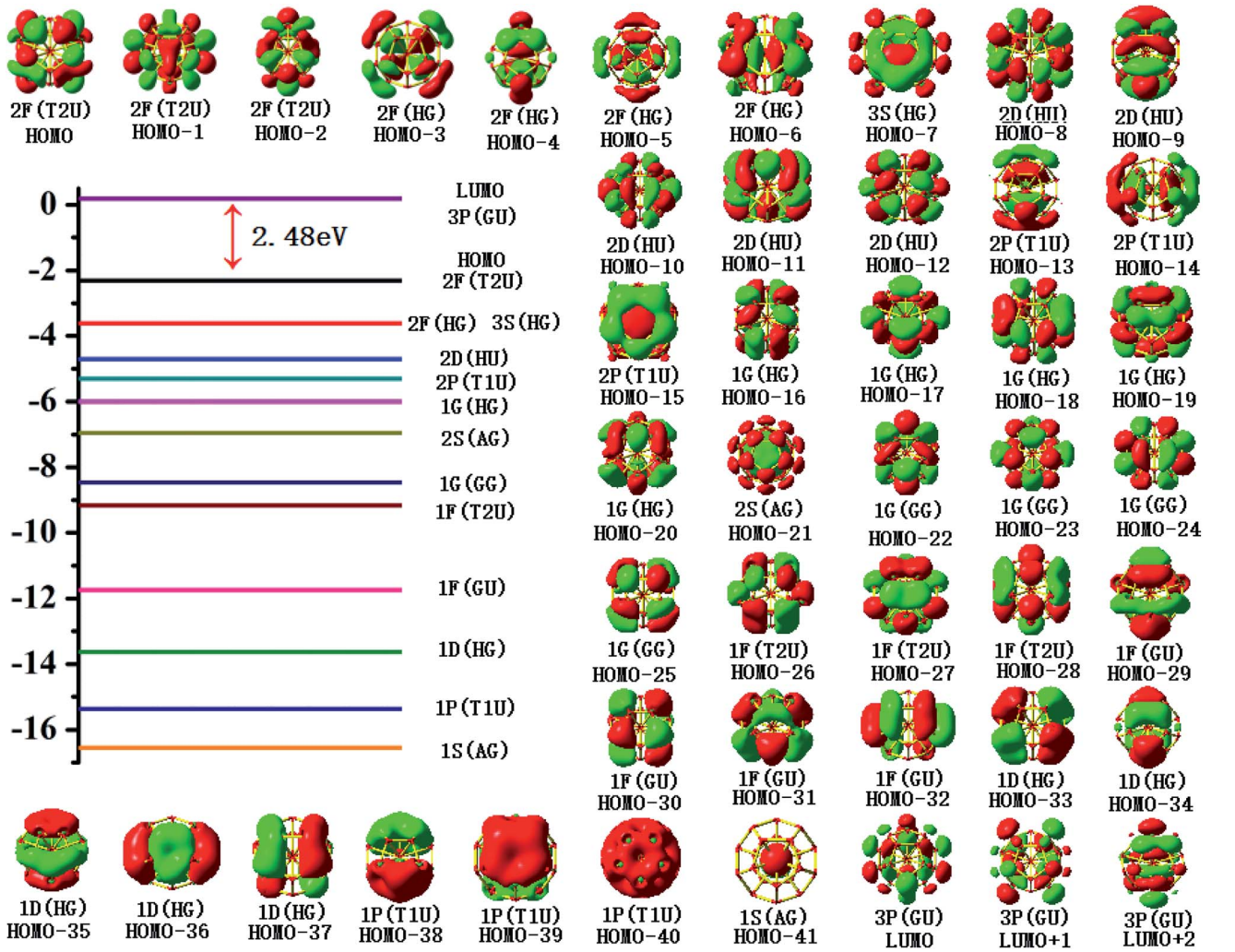

Fig. 5 Molecular orbital maps of the HOMOs and LUMOs of the YSi_{20}^- cluster.

the bonding between the Y atom and Si_{20} shell. As can be seen from Fig. 6, the chemical bonding of 84 valence electrons can be classified into two classes: 2c–2e and 6c–2e. The Si_{20} cages are characterized by thirty 2c–2e localized σ Si–Si bonds with 1.86–1.93 $|e|$ in each bond. The twelve delocalized 6c–2e bonds with 1.95–1.96 $|e|$ in each bond are responsible for the conjugation between the central Y atom and the outer fullerene-shell of Si_{20} and stabilize the encapsulated YSi_{20}^- species.

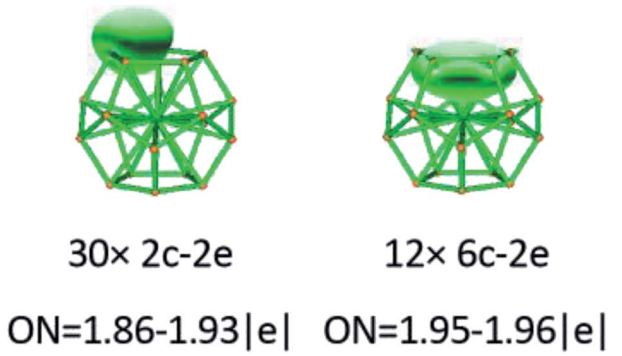

Fig. 6 AdNDP analysis of the YSi_{20}^- cluster. ON stands for the occupation number.

Conclusions

We have achieved a global search for the low energy of neutral and anionic Y-doped Si clusters $YSi_n^{0/-}$ (n = 6–20) by means of the ABCluster structure searching method combined with the mPW2PLYP double-hybrid density functional. Based on the calculated energies and the measured photoelectron spectroscopy data, the true minima of the most stable structures are confirmed. The results showed that the structural growth patterns of YSi_n^- (n = 6–20) are from a Y-linked two subcluster to a Y encapsulated in Si cages, while for the neutral clusters, from a substitutional structure to a linked one, and in the end to the encapsulated structure with the number of Si atoms increasing from 6 to 20. The theoretical adiabatic electron affinity and vertical detachment energy is in good agreement with the experimental values. Analyses of chemical bonding, chemical reactivity, and relative stability indicate that the YSi_{20}^-

has an ideal thermodynamic stability and chemical reactivity in a high-symmetry endohedral I_h structure, which may make it the most suitable building block for novel optical, optoelectronic photosensitive or catalytic nanomaterials.

Conflicts of interest

There are no conflicts to declare.

Acknowledgements

This study was supported by the National Natural Science Foundation of China (Grant No. 21863007, 21263010), by the Program for Innovative Research Team in Universities of Inner Mongolia Autonomous Region (Grant No. NMGIRT-A1603), and by the Natural Science Foundation of Inner Mongolia (Grant No. 2016MS0307).

References

1 A. Grubisic, Y. J. Ko, H. P. Wang and K. H. Bowen, *J. Am. Chem. Soc.*, 2009, **131**, 10783–10790.
2 K. Koyasu, J. Atobe, S. Furuse and A. Nakajima, *J. Chem. Phys.*, 2008, **129**, 214301.
3 K. Koyasu, J. Atobe, M. Akutsu, M. Mitsui and A. Nakajima, *J. Phys. Chem. A*, 2007, **111**, 42–49.
4 A. J. Kenyon, *Semicond. Sci. Technol.*, 2005, **20**, R65–R84.
5 G. H. Cocoletzi, M. T. R. D. L. Cruz and N. Takeuchi, *Surf. Sci.*, 2008, **602**, 644–649.
6 S. Sanna, C. Dues, W. G. Schmidt, F. Timmer, J. Wollschlager, M. Franz, S. Applfeller and M. Dahne, *Phys. Rev. B*, 2016, **93**, 195407.
7 X. X. Xia, A. Hermann, X. Y. Kuang, Y. Y. Jin, C. Lu and X. D. Xing, *J. Phys. Chem. C*, 2016, **120**, 677–684.
8 W. G. Sun, J. J. Wang, C. Lu, X. X. Xia, X. Y. Kuang and A. Hermann, *Inorg. Chem.*, 2017, **56**, 1241–1248.
9 W. G. Sun, X. X. Xia, C. Lu, X. Y. Kuang and A. Hermann, *Phys. Chem. Chem. Phys.*, 2018, **20**, 23740–23746.
10 H. Tsunoyama, M. Shibuta, M. Nakaya, T. Eguchi and A. Nakajima, *Acc. Chem. Res.*, 2018, **51**, 1735–1745.
11 C. Y. Xiao, J. Blundell, F. Hagelberg and W. A. Lester, *Int. J. Quantum Chem.*, 2004, **96**, 416–425.
12 Z. J. Wu and Z. M. Su, *J. Chem. Phys.*, 2006, **124**, 184306.
13 A. P. Yang, Z. Y. Ren, P. Guo and G. H. Wang, *J. Mol. Struct.*, 2008, **856**, 88–95.
14 J. Li, L. Zhang, Z. H. Gao, S. Zhang, C. Lu and G. Q. Li, *Struct. Chem.*, 2016, **27**, 983–992.
15 L. J. Guo, X. H. Zheng, Z. Zeng and C. Zhang, *Chem. Phys. Lett.*, 2012, **550**, 134–137.
16 V. Kumar, A. K. Singh and Y. Kawazoe, *Phys. Rev. B: Condens. Matter Mater. Phys.*, 2006, **74**, 125411.
17 S. Jaiswal, V. P. Babar and V. Kumar, *Phys. Rev. B: Condens. Matter Mater. Phys.*, 2013, **88**, 085412.
18 G. Maroulis, *Int. J. Quantum Chem.*, 2012, **112**, 2231–2241.
19 Y. M. Liu, J. C. Yang and L. Cheng, *Inorg. Chem.*, 2018, **57**, 12934–12940.
20 J. C. Yang, Y. T. Feng, X. H. Xie, H. W. Wu and Y. M. Liu, *Theor. Chem. Acc.*, 2016, **135**, 204.
21 S. He and J. C. Yang, *Theor. Chem. Acc.*, 2017, **136**, 93.
22 L. Y. Hou, J. C. Yang and Y. M. Liu, *J. Mol. Model.*, 2017, **23**, 117.
23 Y. T. Feng, J. C. Yang and Y. M. Liu, *Theor. Chem. Acc.*, 2016, **135**, 258.
24 H. M. Ning, Y. S. Gu, L. Cheng and J. C. Yang, *Chin. J. Struct. Chem.*, 2018, **37**, 854–870.
25 W. Y. Jiang, M. L. Laury, M. Powell and A. K. Wilson, *J. Chem. Theory Comput.*, 2012, **8**, 4102–4111.
26 B. L. Chen, W. G. Sun, X. Y. Kuang, C. Lu, X. X. Xia, H. X. Shi and G. Maroulis, *Inorg. Chem.*, 2018, **57**, 343–350.
27 Y. Y. Jin, G. Maroulis, X. Y. Kuang, L. P. Ding, C. Lu, J. J. Wang, J. Lv, C. Z. Zhang and M. Ju, *Phys. Chem. Chem. Phys.*, 2015, **17**, 13590–13597.
28 J. Zhang and M. Dolg, *Phys. Chem. Chem. Phys.*, 2015, **17**, 24173–24181.
29 J. P. Perdew, K. Burke and M. Ernzerhof, *Phys. Rev. Lett.*, 1996, **77**, 3865–3868.
30 P. J. Hay and W. R. Wadt, *J. Chem. Phys.*, 1985, **82**, 299–310.
31 D. Andrae, U. Häußermann, M. Dolg, H. Stoll and H. Preuß, *Theor. Chim. Acta*, 1990, **77**, 123–141.
32 D. Andrae, U. Häußermann, M. Dolg, H. Stoll and H. Preuß, *Theor. Chim. Acta*, 1991, **78**, 247–266.
33 D. E. Woon and T. H. D. Jr, *J. Chem. Phys.*, 1993, **98**, 1358–1371.
34 T. Schwabe and S. Grimme, *Phys. Chem. Chem. Phys.*, 2006, **8**, 4398–4401.
35 J. Akola, M. Manninen, H. Häkkinen, U. Landman, X. Li and L. S. Wang, *Phys. Rev. B: Condens. Matter Mater. Phys.*, 1999, **60**, R11297.
36 D. J. Tozer and N. C. Handy, *J. Chem. Phys.*, 1998, **109**, 10180–10189.
37 T. Lu and F. W. Chen, *J. Comput. Chem.*, 2012, **33**, 580–592.
38 D. Y. Zubarev and A. I. Boldyrev, *Phys. Chem. Chem. Phys.*, 2008, **10**, 5207–5217.
39 L. S. C. Martins, F. A. L. D. Souza, G. A. Ceolin, F. E. Jorge, R. C. D. Berrêdo and C. T. Campos, *Comput. Theor. Chem.*, 2013, **1013**, 62–69.
40 M. J. Frisch, G. W. Trucks, H. B. Schlegel, G. E. Scuseria, M. A. Robb, J. R. Cheeseman, G. Scalmani, V. Barone, B. Mennucci, G. A. Petersson, H. Nakatsuji, M. Caricato, X. Li, H. P. Hratchian, A. F. Izmaylov, J. Bloino, G. Zheng, J. L. Sonnenberg, M. Hada, M. Ehara, K. Toyota, R. Fukuda, J. Hasegawa, M. Ishida, T. Nakajima, Y. Honda, O. Kitao, H. Nakai, T. Vreven, J. A. Montgomery Jr, J. E. Peralta, F. Ogliaro, M. Bearpark, J. J. Heyd, E. Brothers, K. N. Kudin, V. N. Staroverov, T. Keith, R. Kobayashi, J. Normand, K. Raghavachari, A. Rendell, J. C. Burant, S. S. Iyengar, J. Tomasi, M. Cossi, N. Rega, J. M. Millam, M. Klene, J. E. Knox, J. B. Cross, V. Bakken, C. Adamo, J. Jaramillo, R. Gomperts, R. E. Stratmann, O. Yazyev, A. J. Austin, R. Cammi, C. Pomelli, J. W. Ochterski, R. L. Martin, K. Morokuma, V. G. Zakrzewski, G. A. Voth, P. Salvador, J. J. Dannenberg, S. Dapprich, A. D. Daniels, O. Farkas, J. B. Foresman,

J. V. Ortiz, J. Cioslowski and D. J. Fox, *Gaussian 09, Revision C.01*, Gaussian, Inc, Wallingford CT, 2010.
41 J. C. Yang, W. G. Xu and W. S. Xiao, *J. Mol. Struct.*, 2005, **719**, 89–102.
42 I. Vasiliev, S. öğüt and J. R. Chelikowsky, *Phys. Rev. Lett.*, 1997, **78**, 4805.
43 S. Nigam, C. Majumder and S. K. Kulshreshtha, *J. Chem. Phys.*, 2006, **125**, 074303.
44 X. L. Zhu, X. C. Zeng and Y. A. Lei, *J. Chem. Phys.*, 2004, **120**, 8985–8995.